X-Ray Effects on First Surfaces in the Inertial Confinement Fusion Laboratory Microfusion Facility

Robert R. Peterson

December 1989

UWFDM-818

FUSION TECHNOLOGY INSTITUTE

UNIVERSITY OF WISCONSIN

MADISON WISCONSIN

DISCLAIMER

This report was prepared as an account of work sponsored by an agency of the United States Government. Neither the United States Government, nor any agency thereof, nor any of their employees, makes any warranty, express or implied, or assumes any legal liability or responsibility for the accuracy, completeness, or usefulness of any information, apparatus, product, or process disclosed, or represents that its use would not infringe privately owned rights. Reference herein to any specific commercial product, process, or service by trade name, trademark, manufacturer, or otherwise, does not necessarily constitute or imply its endorsement, recommendation, or favoring by the United States Government or any agency thereof. The views and opinions of authors expressed herein do not necessarily state or reflect those of the United States Government or any agency thereof.

X-RAY EFFECTS ON FIRST SURFACES IN THE INERTIAL CONFINEMENT FUSION LABORATORY MICROFUSION FACILITY

Robert R. Peterson
Fusion Technology Institute
Department of Nuclear Engineering and Engineering Physics
University of Wisconsin - Madison
1500 Johnson Drive
Madison, WI 53706-1687

December 1989

UWFDM-818

1. INTRODUCTION

The target chamber of an Inertial Confinement Fusion (ICF) power plant or of an ICF Laboratory Microfusion Facility (LMF) [1] must survive repetitive blasts from microexplosions of targets. The LMF would explode perhaps as many as 15,000 targets, each with a yield of 1000 MJ, over its 30 year lifetime, and several thousand more at lower yields. A typical ICF power plant design might explode 10^8 targets per year. One challenge of ICF target chamber design is mitigation of the effects of the target generated x-rays on the first surface. The design criteria for the LMF and for an ICF power plant differ significantly. Because of the large number of explosions, the first surface for a power plant must have essentially no vaporization of the solid wall or erosion of the wall will limit the lifetime. Wall erosion is a minor issue for the LMF, so significant vaporization of the first wall material could occur. One consequence of significant vaporization is the launching of shock waves into the solid wall. These vaporization driven shocks are the subject of this paper.

In an LMF target chamber, tens or hundreds of MJ of x-rays will be released by the burning target over a pulse width of a few ns. If x-ray absorbing structures or gases are placed between the target and the first wall, then the energy of the x-rays can be reradiated to the wall over a time that is long compared to the thermal response time of the wall and vaporization of the surface of the wall may be avoided. A gas of high enough density and atomic number may prevent the propagation of the driver beam, though there may be solutions to this problem as well. In the absence of something to absorb the target generated x-rays, the x-ray power intensity on the first wall will be high enough to vaporize the first wall surface.

I will begin this paper with a study of the response of LMF first walls to target x-rays. I have used computer simulations and analytic models to study the effect of the x-ray pulse width on the strength of shock waves in the wall material. I will also show the results of computer simulations of possible experiments to mimic the x-ray damage to potential first wall materials. I will then discuss such experiments done using x-rays from gas pinches generated on the SATURN accelerator at Sandia National Laboratories (SNL) in Albuquerque, New Mexico. Finally, I will discuss the fragmentation of structures inside the target chamber by the x-rays.

2. FIRST WALL

I have studied the response of LMF target chamber walls to direct irradiation by target x-rays. I have tried to develop analytic scaling laws to predict the pressures generated in the first wall materials by the absorption of x-rays. This is useful in understanding the physics of shock wave generation and because computer simulations can be expensive and time consuming so that simulations for every conceivable set of parameters is not practical. Scaling laws must be normalized and require simplifying assumptions, so I have combined this analytic treatment with computer simulations. In this way I have studied the effect of x-ray pulse width and of the vaporization process on the strength of shocks generated in first wall material.

2.1 Physical Models and Analytic Treatment

The first wall responds to target x-rays through very rapid energy deposition in a thin layer of material. This leads to volumetric vaporization of from a few to a few tens of microns of material and the generation of shock waves moving into the material. The volumetric vaporization has been a topic of study for several years [2] and will not be discussed in this report. I will concentrate on the generation of shocks.

Shocks are launched in the material by x-ray generated pressure profiles. In a solid or a gas, the pressure is proportional to the energy density. For an ideal gas, this proportionality constant is 2/3, while in a solid this constant is the Grueneisen coefficient Γ, typically about 2 for metals under standard conditions [3]. Therefore, one can express the x-ray generated pressure in terms of the x-ray deposited energy density in the material. If we assume that the energy is spread over a thickness Δx in the material and that the energy fluence is

$$F_X = I_X \, \Delta t \, , \tag{1}$$

then one can write the pressure as,

$$P = A \, F_X / \Delta x \, . \tag{2}$$

Here, I_X is the x-ray power intensity on the material in power per unit area, Δt is the x-ray pulse width, F_X is the x-ray energy fluence, and A is a proportionality constant. The energy spreads through the material after deposition at 1 to a few times C_S, the speed of sound, and therefore Δx is the greater of the deposition length of x-rays in the material and $BC_S\Delta t$, where B is a constant of order of a few that is dependent on the shock strength. In this study, I have concentrated on aluminum and graphite, which have cold sound speeds of 6.5 and 2.5 km/s respectively. According to the LANL shock data [4], for shock pressures between 10 and 100 GPa the shock speed is 2 to 4 times C_S for graphite ATJ and 1 to 2 times C_S for aluminum 6061. These numbers are representative of the LMF. I have considered pulse widths from 1 to 40 ns, so the x-ray energy can hydrodynamically spread from about 5 microns to about 400 microns, depending on the shock strength and pulse width. The x-ray deposition length of 1 keV x-rays in aluminum is 3.1 microns and in graphite, at a density of 1.77 g/cm^3, is 2.8 microns [5]. So for all but the shortest pulses, hydrodynamic motion is the dominant effect in determining Δx. Therefore,

$$P = A \, I_X / B \, C_S \, . \tag{3}$$

The true sound speed in a gas increases with temperature, and therefore increases with I_X. Therefore, as long as the material is behaving hydrodynamically like a gas, the pressure could be expressed as

$$P = C\, I_x^n\,, \tag{4}$$

where C is a constant and n is a real number, probably slightly below 1.0. Computer simulations in the next section further study the dependence of the pressure on the power intensity by predicting the peak pressures for a constant energy fluence but for different pulse widths.

2.2 Computer Simulations

An important aspect of this investigation of x-ray vaporization is computer simulation. I have used two different sets of computer codes in this, which have compensating strengths and weaknesses. I have used these codes to consider x-ray vaporization in ICF target chambers. Part of this has been to study the dependence on x-ray power suggested in section 2.1. Finally, I have used computer simulations to help design and understand x-ray vaporization experiments.

2.2.1 Computer Codes

I have used two different sets of computer codes to study the launching of shocks by intense x-ray deposition and the subsequent propagation of these shocks into the material. The first set is the IONMIX code [6] coupled to the CONRAD code [7]. These were developed and are being maintained at the University of Wisconsin. CONRAD is a one-dimensional Lagrangian hydrodynamics code with multigroup radiation diffusion. Equations-of-state and multigroup opacities are provided by the IONMIX code in tables. CONRAD includes time-dependent x-ray and ion sources and models energy deposition, thermal conduction, and phase transition in a solid or liquid wall. CONRAD has the advantage that one can directly calculate the mass of material vaporized, which is important both to target chamber design and to validation of the physical models assumed in the vaporization process. The heats of melting and vaporization can be a significant part of the energy budget and care has been taken to include them in CONRAD. In codes designed for use at higher energy densities, the heats of melting and vaporization are only included through the equation-of-state tables, and one is often not sure of the details. The other set is a radiation hydrodynamics code coupled to CSQ. I have used the radiation hydrodynamics code to simulate the deposition of x-rays in the material. This calculation is then coupled to the CSQ computer code. CSQ is a code written and maintained at SNL, that uses two-dimensional Eulerian hydrodynamics and has sophisticated modeling of phase transitions and crush physics that are probably important to shock attenuation in materials [8]. CSQ has rather limited radiation transport modelling, which makes such coupling to another computer code advisable when doing x-ray vaporization simulations.

2.2.2 First Wall Simulations

I have used these computer codes to simulate the responses of LMF first walls to the direct deposition of target x-rays. We have used LMF concepts devised both at SNL, applicable to light ion driven fusion, and Lawrence Livermore National Laboratory (LLNL), more tied to laser driven inertial fusion. The parameters used for the calculations and the results are summarized in Table 1. The SNL concepts often require a short distance between the last elements in the beam generation hardware and the target. The present baseline design invokes ballistic focussing of the ions with lens magnets [9]. The beam divergence places an upper limit on the distance between the lens and the target, which is currently believed to be 150 cm. The first wall of the target chamber is placed at the lens position. LLNL concepts using lasers have the final driver components many meters from the target, so there is greater freedom in positioning the first wall of the target chamber. I have considered wall radii of 4 and 5 m, respectively for calculations #4 and 5. For all calculations I have assumed that the target is releasing 220 MJ of x-rays from a total yield of 1000 MJ in 1 ns. I assume that the x-ray spectrum is as shown in Fig. 1. These are all consistent

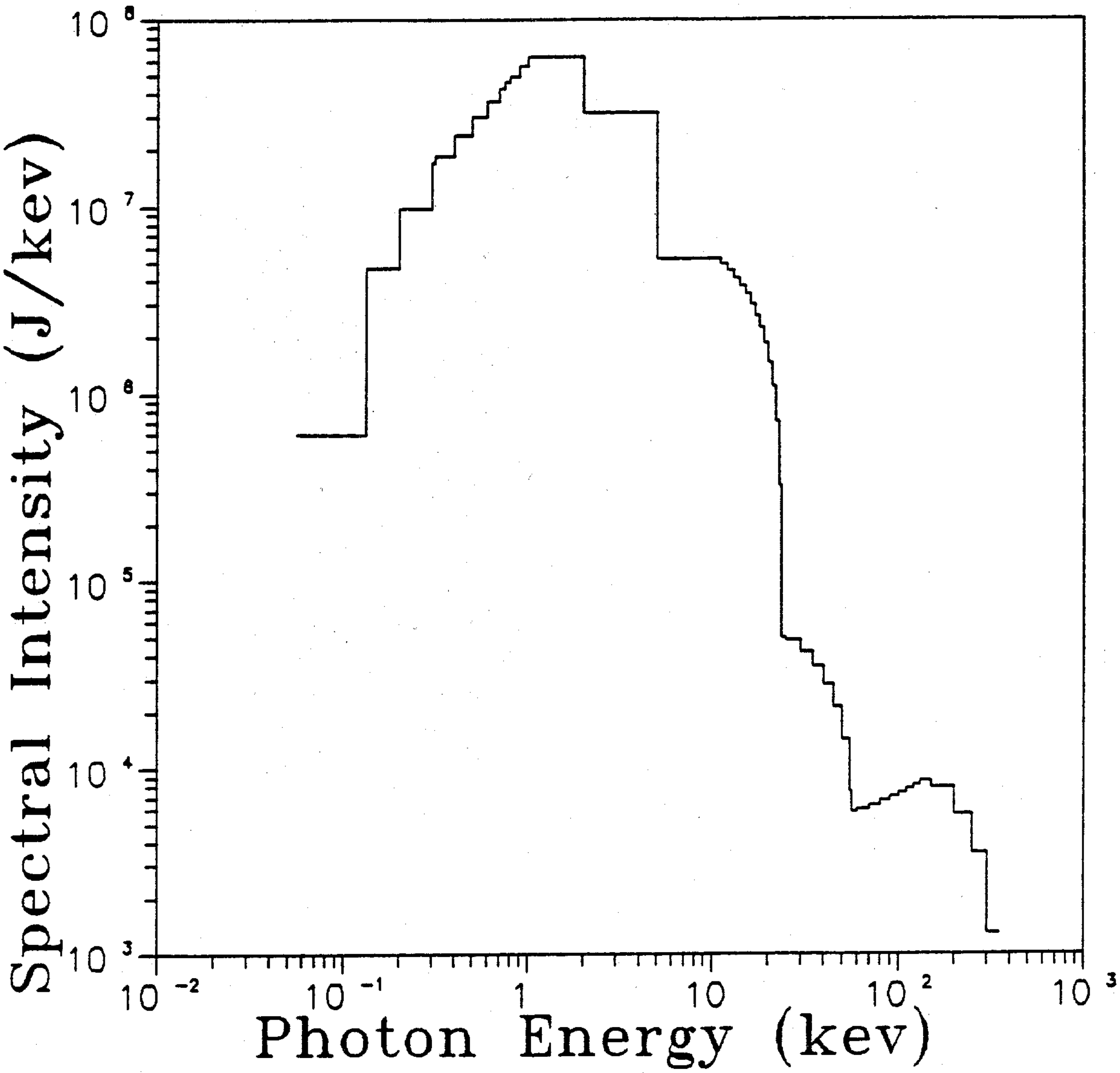

Fig. 1. HIBALL target x-ray spectrum.

with the HIBALL target [10] and there will be some variation from this in the LMF due to different target designs.

Table 1. X-Ray Vaporization in LMF First Walls

Calculation #	1	2	3	4	5
Code	CONRAD	CONRAD	CSQ	CSQ	CONRAD
Concept	SNL	SNL	SNL	LLNL	LLNL
X-Ray Fluence (J/cm^2)	780	780	780	70	110
Wall Material	Al	C	Al	Al	Frost
Vaporized Mass (kg)	2.8	1.8	*	*	12.6
Peak Pressure in Vapor (GPa)	150	84	*	50	1.2
Peak Pressure in Wall (GPa)	122	94	45^{t}	7.2^{tt}	0.65
Impulse on Wall (Pa-s)	310	257	300^{t}	100^{tt}	90.2

* Not Calculated
^{t} 5x10^{-3} cm in back of surface
^{tt} 5x10^{-2} cm in back of surface

One can infer some trends from the results in Table 1, though I will not discuss the five computer simulations of Table 1 in detail at this time. Calculations 1 and 3 are a comparison of CONRAD and CSQ for the same problem. In the CSQ runs, the mass of vaporized material is not calculated. Also for calculation #3, I have no reliable value for the peak pressure in the vaporized material. The peak pressure 50 microns in back of the aluminum surface as calculated by CSQ is 37% of the value on the surface as calculated by CONRAD. This is most likely due to attenuation of the shock passing through 50 microns of solid and an increase in the pressure calculated on the wall in the CONRAD run because the wall surface is artificially held fixed so the shock reflects, leading to an increase in the pressure on the wall. The two simulations agree in their estimation of the total impulse on the wall, which gives one some confidence in these simulations. Calculation #2 is for a graphite lined SNL LMF. The vaporized mass, peak pressure in the vapor, the peak pressure on the wall, and the total impulse are all reduced for graphite, compared to aluminum. When one compares calculations 3 and 4, one sees the effects reducing the energy fluence by a factor of ten for the same wall material. The peak pressure in the wall at 500 microns, which is not given in Table 1, is about 14 GPa for calculation #3, compared with 7.9 GPa for #4. The impulse is reduced by a factor of 3. Calculation #5 shows the beneficial effects of both reducing the fluence and choosing low density frost as a first wall material. The low density, ρ = 0.1 g/cc, spreads out the energy over a larger volume and thus reduces the pressure in the vaporized matter. The total impulse is reduced slightly.

It is somewhat difficult to compare the results of CONRAD and CSQ simulations because the CSQ results are shown as stresses in the material. One of the strengths of CSQ is that one can include the proper physics that leads to attenuation of the shock in the material. In Fig. 2 we show how CSQ predicts the stress or pressure, recorded at various positions in the material as functions of time. For most of my simulations, I use the terms stress and pressure interchangeably because the stress, as calculated by CSQ, is isotropic. CSQ simulations have shown that once the stress level is comparable to the material strength, the stress can become nonisotropic. Figure 2 was part of calculation #4 in Table 1. One sees as one moves from 0.05 cm to 0.15 cm to 0.25 cm in back of the surface, the stress drops from 75 kbar to 30 kbar to 15 kbar. CSQ calculations have shown that at a certain point in the material, the stress no longer drops as one moves farther into the material and that value of the stress is a function of the x-ray energy fluence and not the pulse width. As I will discuss in section 2.2.3, the stress nearer the surface is a function of the pulse width.

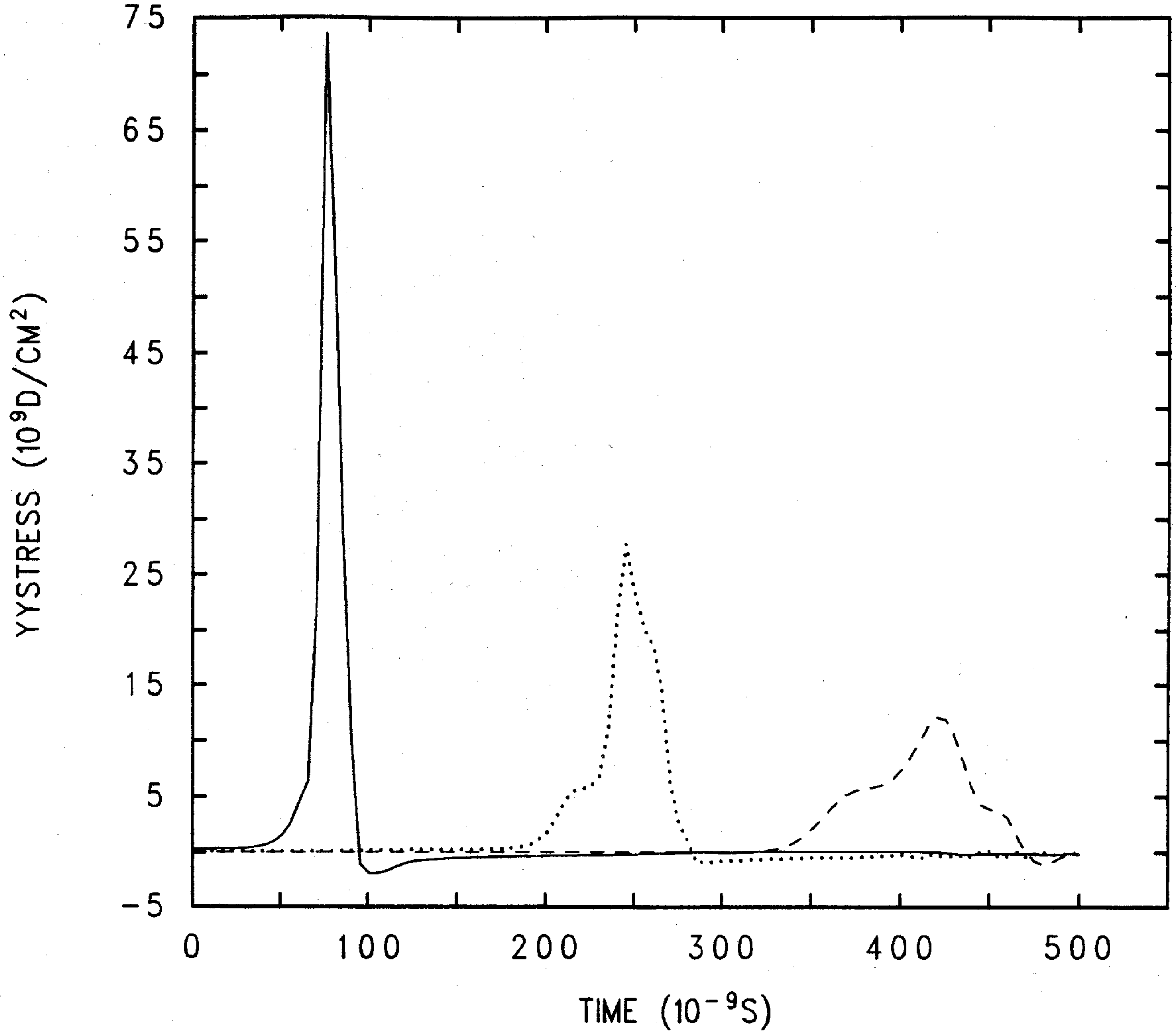

Fig. 2. Stress versus time at various positions in the material. This calculation is for an aluminum wall 5 meters from a 1000 MJ target explosion.

In Table 2, I display the results of several CONRAD calculations where I have run the calculations with and without the effects of vaporization. I ran CONRAD in two modes: 1) material that has sufficient energy density to vaporize gives up the heat of vaporization and then moves as a fluid, while the rest of the wall material does not move, and 2) all matter can move, but no energy is lost to the heat of vaporization and no strength of material effects are considered on the motion. I ran calculations for the SNL parameters with aluminum and graphite first walls and for the LLNL H_2O frost concept. In Fig. 3, I show the positions of Lagrangian zone boundaries in a CONRAD simulation for the frost concept. In this calculation, all of the zones are allowed to move as in mode 2. I calculated in a similar CONRAD simulation that was run in mode 1, with vaporization, what part of the frost remains unvaporized, which is shown in the figure as cross-hatched. Here one can see that the shock continues into the unvaporized part of the frost. One can easily explain why the peak pressure in the vapor for the frost concept is higher when vaporization is not included; there is a lot of energy lost to vaporization. I am still studying why the trend is reversed at high fluence and for aluminum and graphite.

2.2.3 <u>Response Versus Pulse Width</u>

I have tested the scaling of pressure with x-ray power with computer simulations. In Table 3, I show the results of CONRAD simulations with the effect of vaporization in effect as described in the previous section. In all the calculations, the x-ray fluence is 780 J/cm^2 and the spectrum is as in Fig. 1. Only the pulse width of the x-rays on the wall is varied. One can see that the vaporized mass and the total impulse are not much affected by the pulse width. However, the peak pressure on the wall is very much affected. In Fig. 4, we have graphically displayed this dependence. I have proposed a scaling law,

$$P = P(\Delta t = 1 \text{ ns}) / \Delta t^n , \tag{5}$$

Table 2. Comparison with and without Vaporization

Calculation	1	2	3	4	5	6
Material	Al	Al	C	C	H_2O	H_2O
Vaporization	Y	N	Y	N	Y	N
X-Ray Fluence (J/cm^2)	780	780	780	780	110	110
Peak Pressure in Vapor (GPa)	150	43	84	61	1.2	3.6
Peak Pressure on Wall (GPa)	122	20.5	94	21	.65	1.5
Impulse on Wall (Pa-s)	310	60	182	120	90	75

Table 3. Response of Material versus Pulse Width

Calculation #	Pulse Width (ns)	Wall Material	Vaporized Mass (kg)	Peak Wall Pressure (GPa)	Impulse on Wall (Pa-s)
1	1	Al	2.839	122	309
2	10	Al	2.749	30	309
3	20	Al	2.746	22	274
4	40	Al	2.822	12	248
5	1	C	1.751	94	257
6	10	C	1.808	23	254
7	20	C	1.743	13	259
8	40	C	1.623	6.4	220

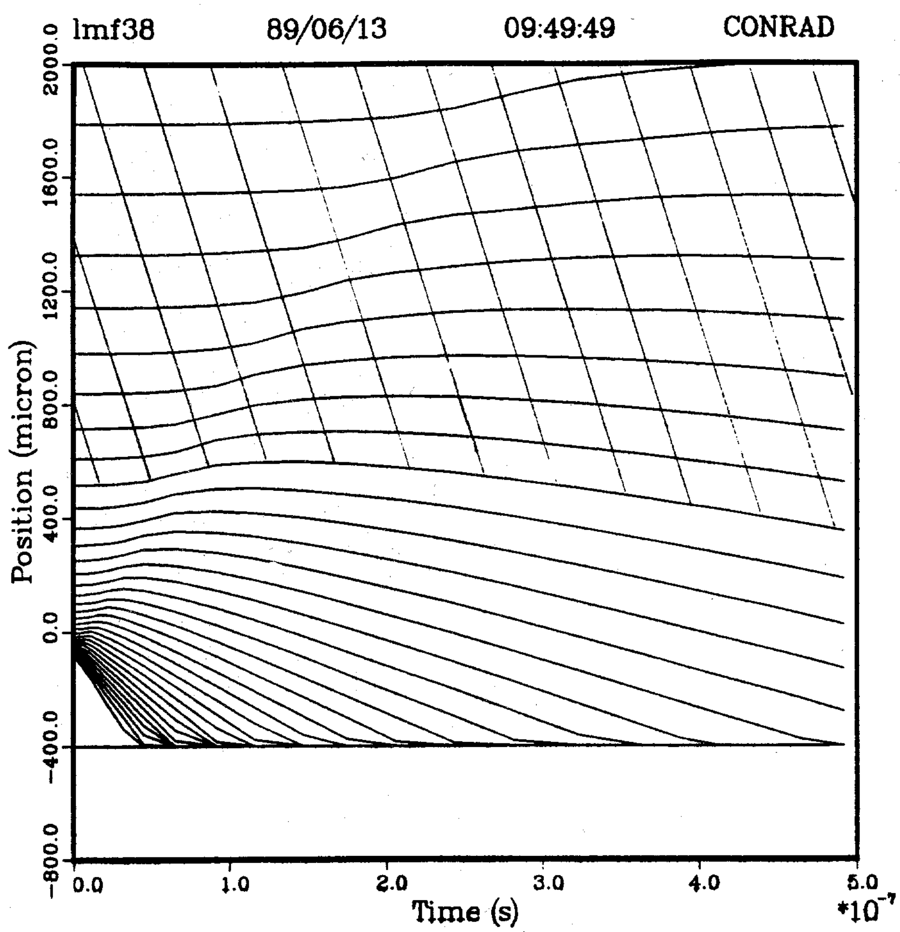

Fig. 3. Hydromotion in water frost on LMF first wall. The calculation was done with CONRAD with all zones free to move and vaporization and the strength of the material is neglected. The hatched region is material that is not vaporized by x-rays, as predicted by a CONRAD calculation where vaporization is considered.

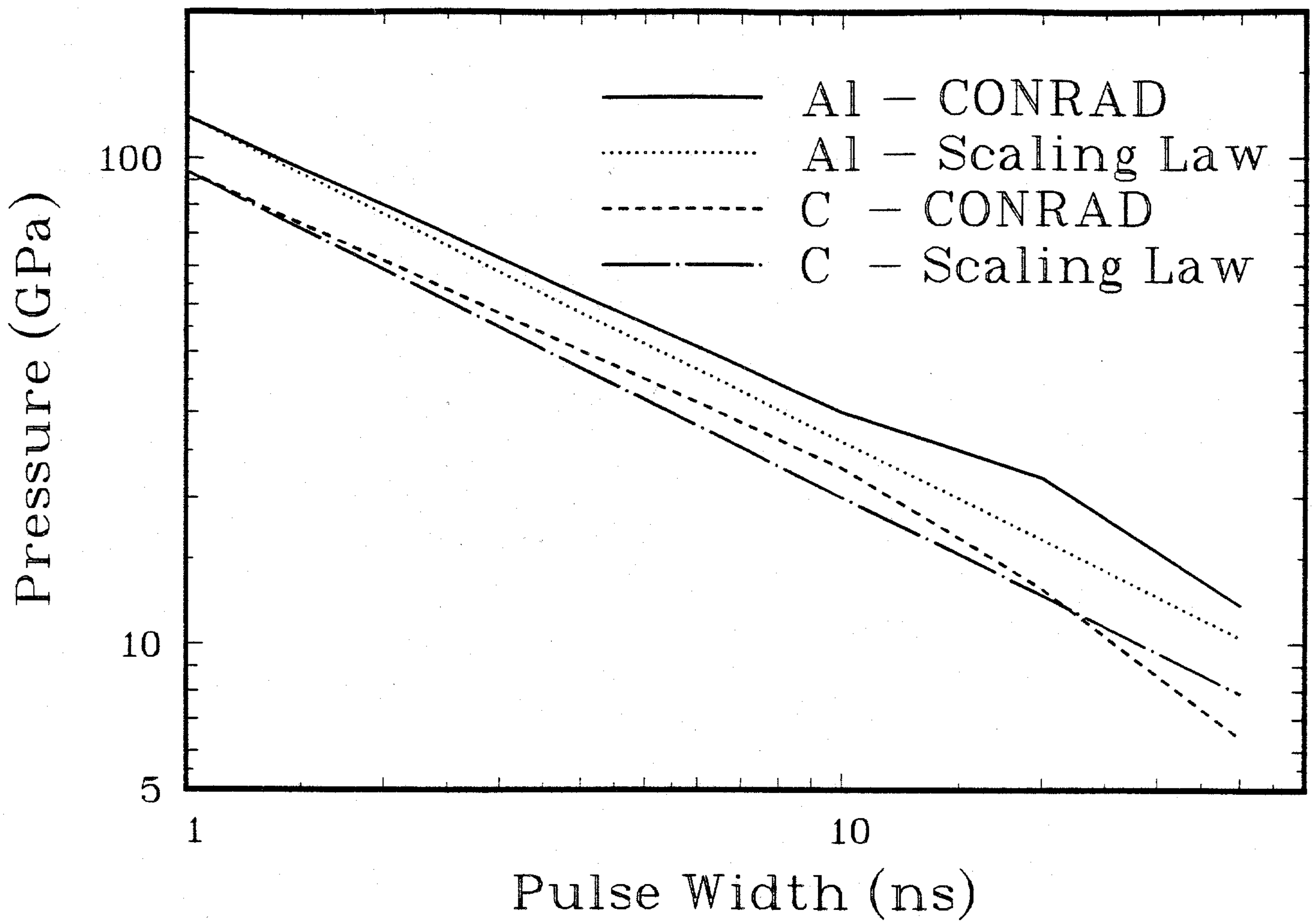

Fig. 4. Pressure on aluminum and graphite walls versus x-ray pulse width. The energy fluence is 780 J/cm^2 and the calculations were done with CONRAD. Scaling laws are also shown.

where P is the peak pressure, Δt is the pulse width, and n is some real number. I have also plotted this scaling law for n = 2/3, and one can see that there is a reasonable fit.

I have also looked at the dependence on pulse width of the peak pressure inside the material with CSQ simulations. The results of these simulations are shown in Fig. 5. One can see that, as one considers the pressure at greater distances from the surface, the dependence on the pulse width becomes weaker. Therefore, whether the x-ray pulse width is important becomes a question of whether or not one is interested in the material response near the surface. The issue of pulse widths can be important when considering experiments to simulate the response of LMF first wall materials, which is the topic of the next section.

2.2.4 Simulation of Experiments

I have used CSQ to study how sample first wall materials might behave in experiments that mimic target chamber x-ray conditions. I have done such computer calculations for samples of aluminum, a thin layer of alumina on aluminum, and graphite. Parameters for three experimental environments are shown in Table 4 along with LMF conditions for SNL and LLNL concepts, where in all cases the wall or sample material is aluminum. PROTO-II is an electron accelerator at SNL that has been used for a number of years to create pulses of x-rays with gas pinches [11]. Specifically, gas puff pinches of neon produce the spectrum shown in Fig. 6 [12]. When one compares this spectrum with the HIBALL target spectrum in Fig. 1 one notices both have peaks at about 1 keV in photon energy. One must also compare the time dependence of the pinch generated x-rays to what the target emits, which has been done in Fig. 7. Here one sees that the HIBALL target emits x-rays over a period of 1 to 2 ns, while a neon gas pinch radiates 1 keV x-rays over 15 to 20 ns and lower energy photons over 100 ns. The experimental arrangement is shown in Fig. 8. The pinch is created in the

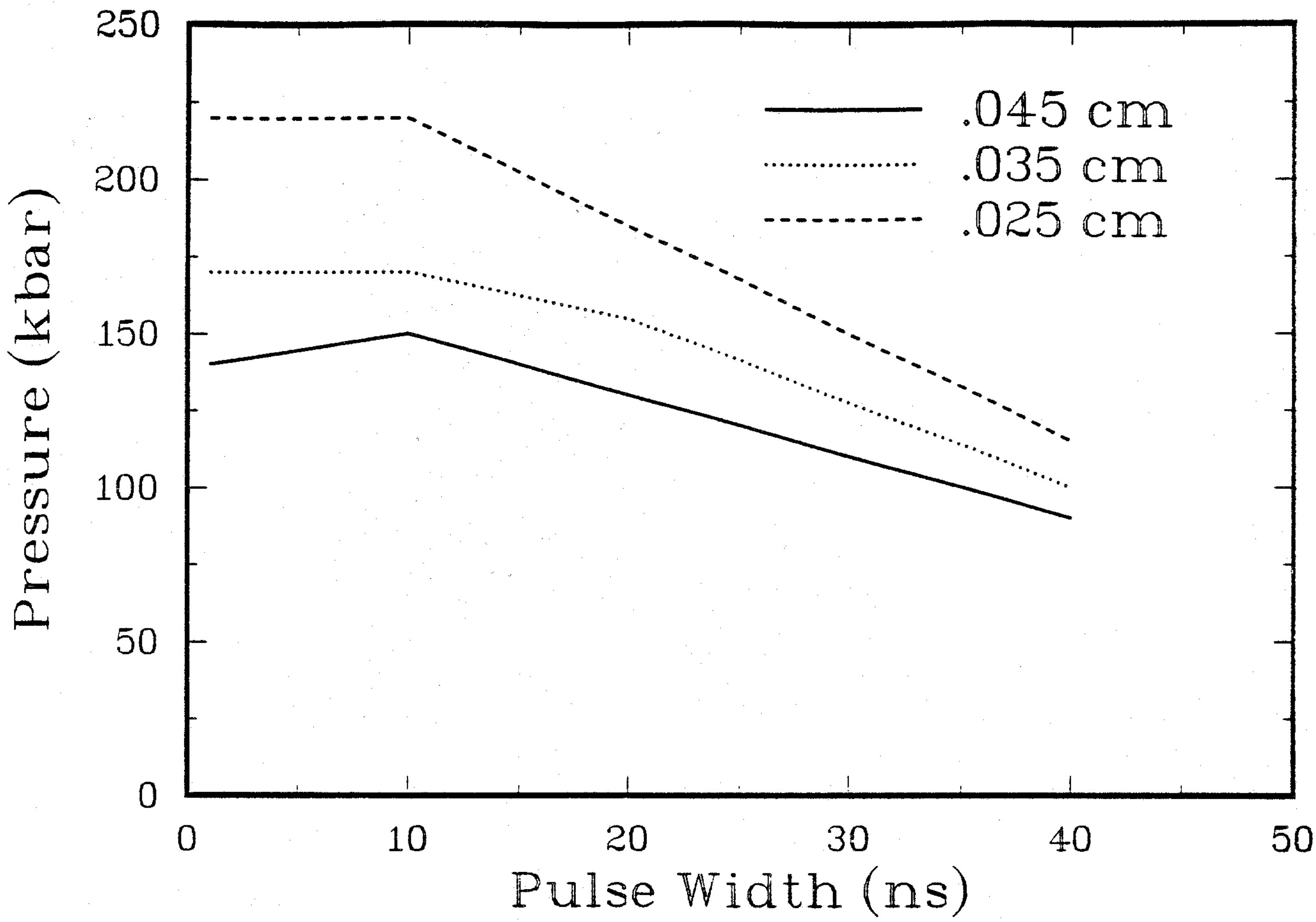

Fig. 5. Stresses at various positions in an aluminum wall versus x-ray pulse width. The energy fluence is 780 J/cm^2 and the calculations were done with CSQ.

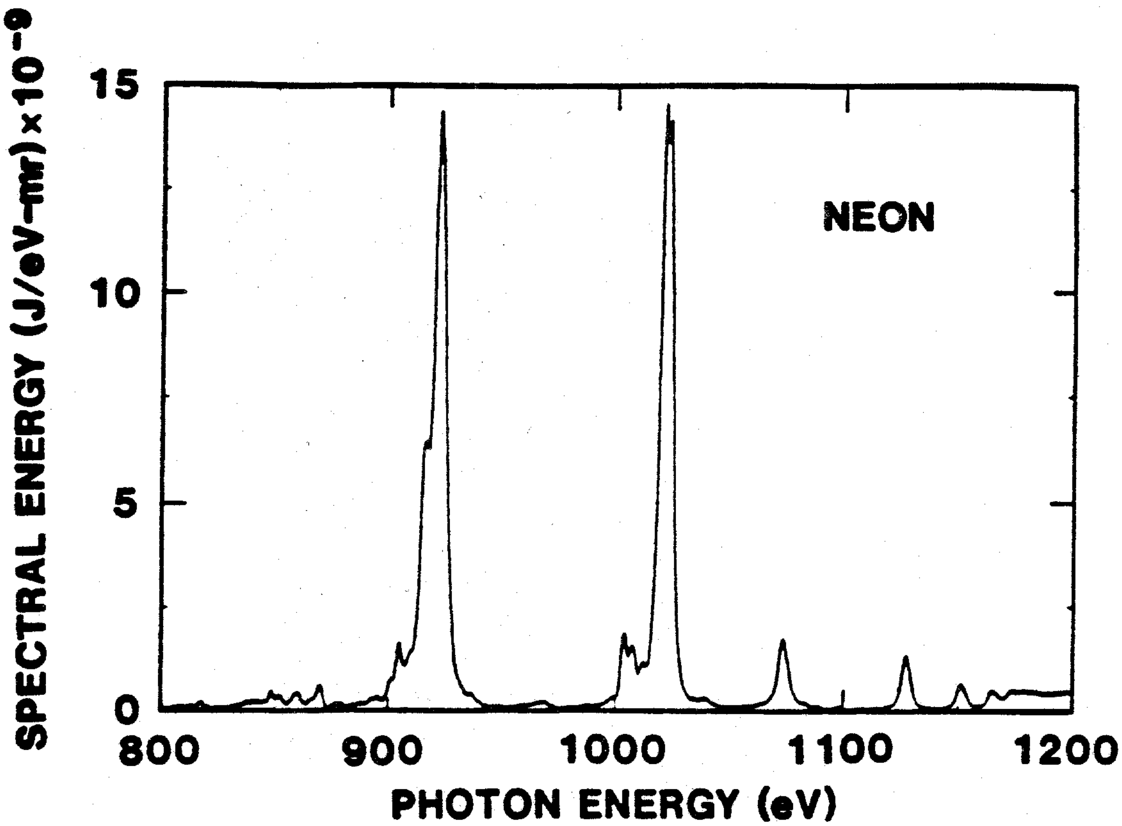

Fig. 6. X-ray spectrum from a neon gas pinch on PROTO-II. Only the component above 900 eV in photon energy is shown. There is another component to the spectrum below a few hundred eV that has about 4 times the energy but more than 5 times the pulse width.

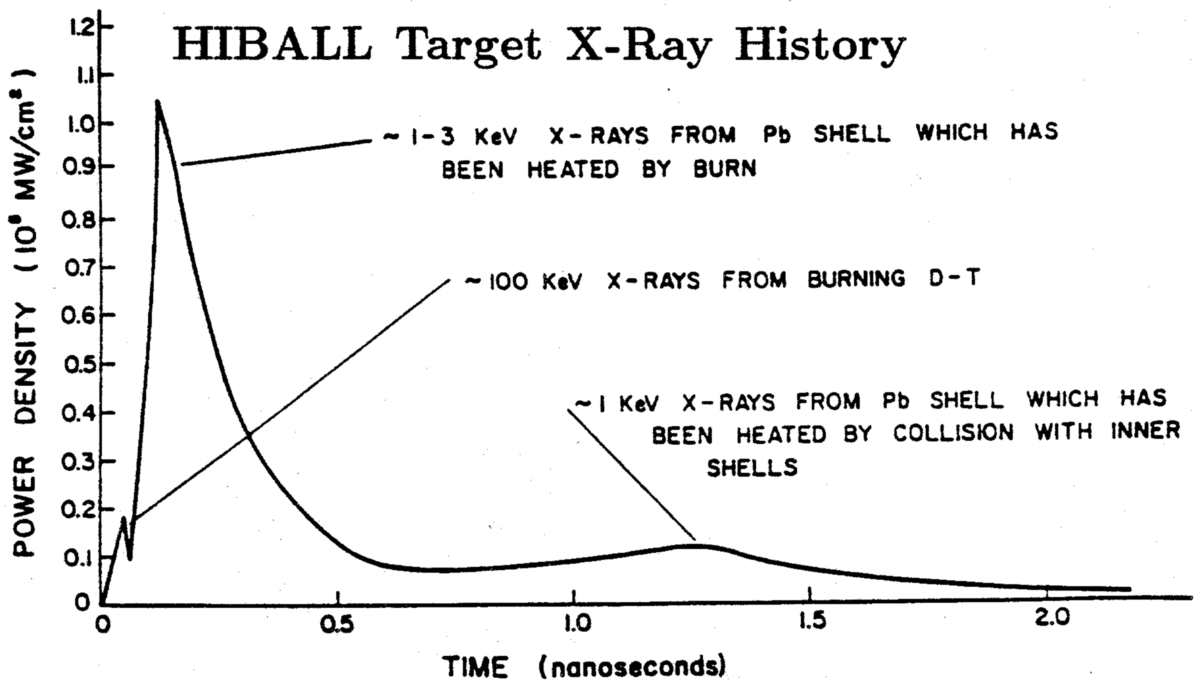

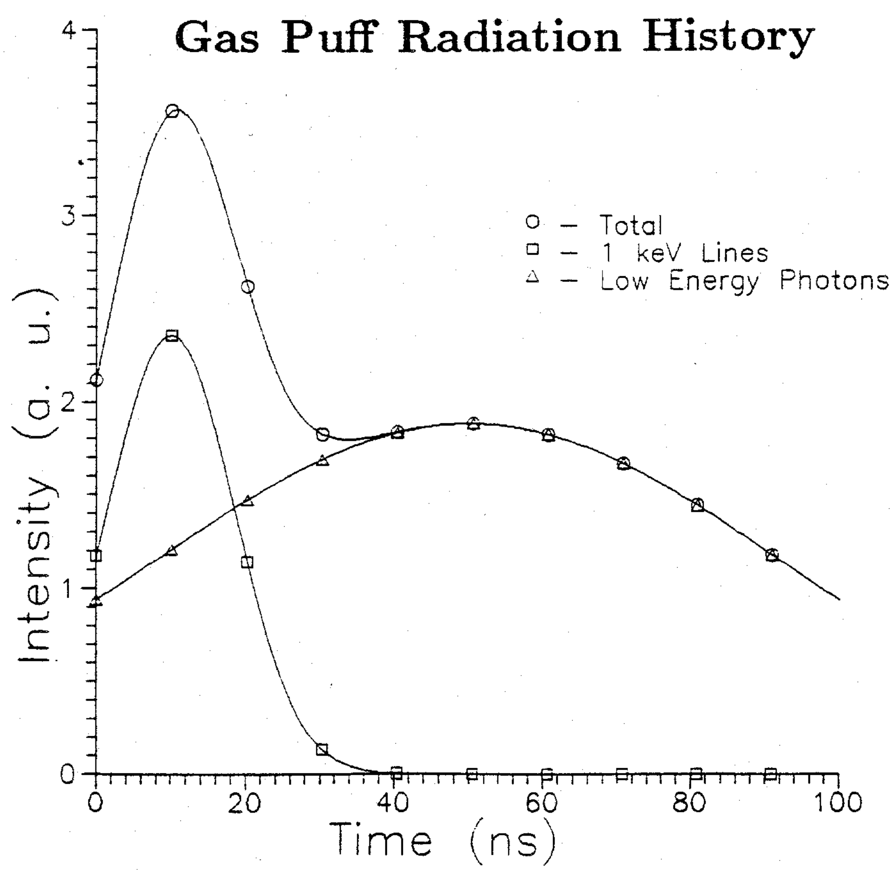

Fig. 7. Time dependence of x-rays emitted from HIBALL target and from a neon gas pinch.

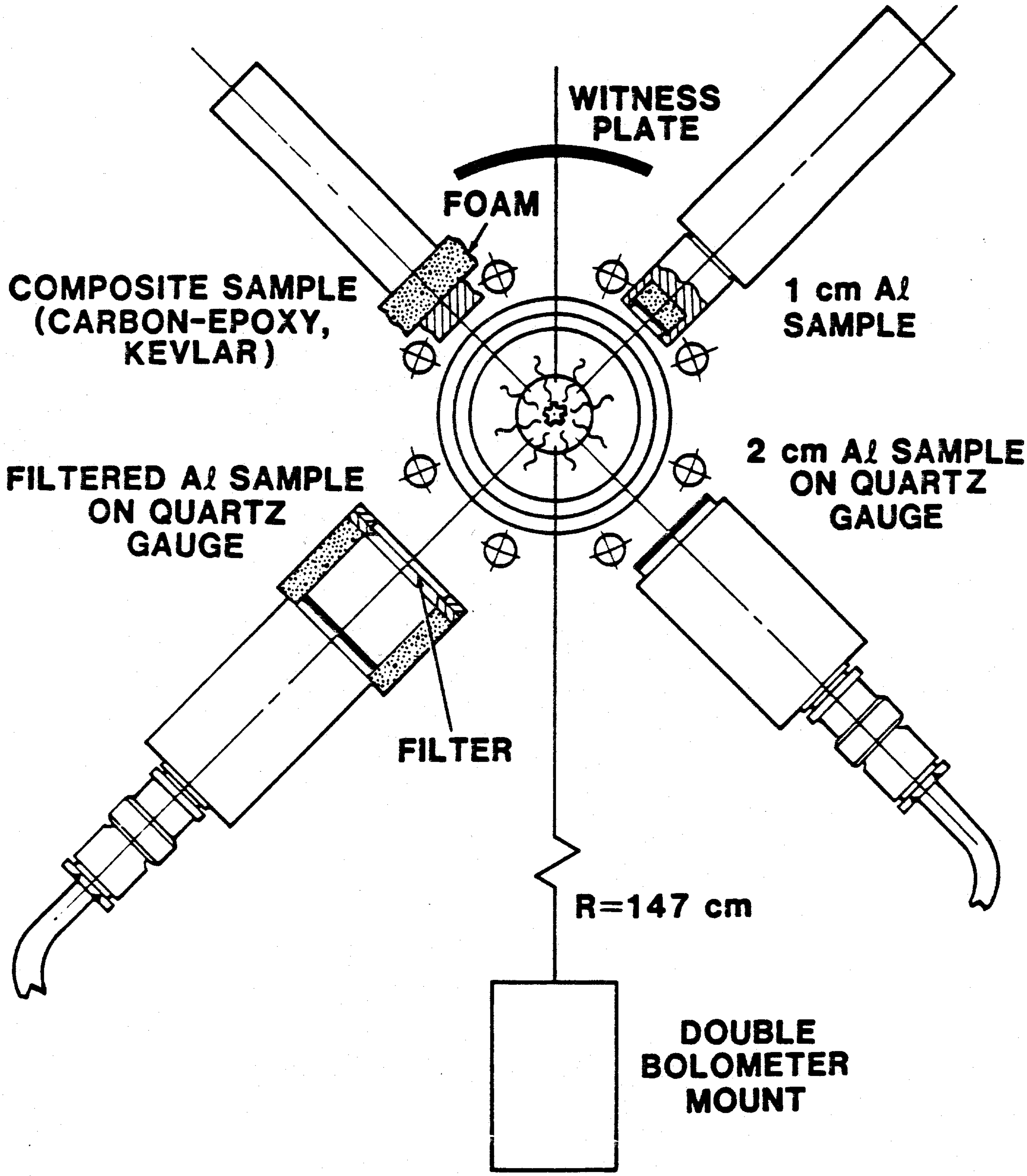

Fig. 8. Schematic picture of experimental arrangement in PROTO-II.

Table 4. X-Ray Driven Stresses in Aluminum

	PROTO-II (gas pinch)	SATURN (gas pinch)	GAMBLE-II (ions)	LMF/LLNL	LMF/SNL
Range in Al (mg/cm^2)	0.83(1)	0.83(1)	3.9(2)	0.83(1)	0.83(1)
X-Ray Energy (MJ)	0.008	0.100	0.017	220	220
Distance (cm)	3.8	3.8	N.A.	500	150
Energy Fluence (J/cm^2)	42	550	400	68	780
Energy Density (kJ/g)	51	660	108	82	940
Pulse Width (ns)	20	15	43	1	1
Power Intensity (GW/cm^2)	2.6	37	9.3	68	780
Power Density (GW/g)	2.5	44	2.5	82	940
Calculated Stress (@ 0.05 cm) (GPa)	1	7.5	not calculated	7.5	14

(1)Assuming 1 keV photons

(2)Assuming 1 MeV protons and no range shortening

center of a circle of current return posts and the closest that a sample can be placed to the x-ray source is just outside these posts. SATURN is a machine similar to PROTO-II at SNL except that it is much larger and only fired its first gas pinches in late 1988. Experiments on SATURN have a very similar arrangement to those in PROTO-II. GAMBLE-II is a machine at NRL that can accelerate protons in a beam to simulate x-ray deposition. One should note that the pulse width of the ion beam on GAMBLE-II is more than 40 ns while the gas pinch x-ray sources have less than half the pulse width. If one is only interested in stresses in the center of the material so that the energy density is important, then experiments on all three machine can be relevant to the LMF. If, however, stresses near the surface are important, the power density (power deposited per unit mass) is the important parameter and only SATURN can do LMF relevant experiments. Even SATURN can only provide a power at one half the LLNL LMF value. The most direct measure is the achievable stress in the material, which I have calculated with CSQ for PROTO-II, SATURN, and SNL and LLNL versions of the LMF. In aluminum, PROTO-II can provide stresses of 1 GPa 0.05 cm in back of the first surface and SATURN can provide 7.5 GPa. I have not yet calculated the stresses that GAMBLE-II could generate in aluminum, though based on the power density one would expect about 1 GPa. I calculated the stresses in a LLNL and SNL LMF aluminum wall to be 7.5 GPa and 14.0 GPa respectively. The calculation of the PROTO-II stresses was rather interesting because here the stresses are only a factor of a few larger than the yield stress and the stresses are nonisotropic. The longitudinal stresses at 0.05 cm peaked at 1.0 GPa while the transverse stresses peaked at 0.7 GPa. These simulations show that experiments on SATURN have the potential to much more closely mimic the conditions in the LMF target chamber than do experiments on GAMBLE-II or PROTO-II.

I have simulated the response of four different materials to x-rays from SATURN with CSQ. The results are summarized in Table 5. In all cases, the samples are assumed to be 3.8 cm from the pinch, which is assumed to generate 100 kJ of x-rays in the lines shown in Fig. 6. There is assumed to be another 400 kJ in x-rays below about 200 eV in photon energy, making a total of 500 kJ in x-rays. I have assumed that the x-rays above 900 eV are emitted in 20 ns in these simulations and that the low energy component is radiated over 100 ns, as shown in Fig. 7. I have done simulations for aluminum, graphite and aluminum coated with a 100 micron thick layer of alumina.

Table 5. Stresses in Various Materials Generated with SATURN X-Rays

	Aluminum (unfiltered)	Graphite (unfiltered)	Graphite (filtered)	Alumina/Aluminum (unfiltered)
Range of 1 keV x-rays (mg/cm^2)	0.83	0.50(1)	0.50	0.38
Mass Density (g/cm^3)	2.7	1.7	1.7	3.5
Energy Fluence (J/cm^2)	550(2)	2750	550	550(2)
Energy Density (kJ/g)	660	5500	1100	1440
Power Density (GW/g)	44	367	73	96
Calculated Stress @ 0.05 cm (GPa)	7.5	36.0	10.2	3.5
Calculated Stress @ 0.15 cm (GPa)	4.8	12.5	5.0	1.8
Calculated Stress @ 0.25 cm (GPa)	2.7	8.0	N.A	1.0

(1) The ranges of 1 keV and 300 eV x-rays in carbon are the same. The range of 100 eV x-rays is 0.05 mg/cm^2.

(2) Because of the much shorter range of low energy photons, the part of the spectrum below 900 eV is ignored and is not included in the energy fluence.

I have considered the effects of these low energy photons. I have done simulations where these photons are filtered out, perhaps with an aluminum foil, and where they are allowed to irradiate the sample. The ranges of 200 eV x-rays in aluminum and alumina are more than an order of magnitude less than the ranges of 1 keV x-rays and should be mostly absorbed in the blowoff plasma and not contribute to the launching of a shock in the material. Therefore, I only show results for these materials where the low energy photons have not been filtered out; the results with filtering are essentially the same. This is not the case for graphite because the range of 200 eV x-rays is only a little shorter than that for 1 keV x-rays. Both unfiltered and filtered simulations are shown for graphite.

Except in the case of alumina on aluminum, one can see that the stress increases with energy density and power density. The stress is recorded at three positions in the material, and one sees that the shock is attenuated in all cases. In the case of alumina on aluminum, the calculated stresses are much lower than the energy and power would predict. There is a mismatch in the speed of sound, mass density, and material strength at the alumina/aluminum interface. This leads to poor transmission of the shock across the interface and a great reduction of the shock strength in the aluminum, where the calculated stress is measured.

3. EXPERIMENTS ON SATURN

During May 1989, I fielded some x-ray vaporization experiments on SATURN like those described in the previous section. All of the samples were donated by LLNL or SNL. The space on the machine was just what remained on experiments that were already planned. The exception to this was shot 669 which only had my samples on it and was donated by SNL. I did not have any active diagnostics to measure the stress levels. The sample holders were loaned to me by other experimenters at SNL. The samples were held in stainless steel 316 Swaglok fittings that held the samples in place with an annular lip. The backs of the samples were supported with carbon foam that was, in turn, supported with a thin aluminum disk. I am still in the process of analyzing these experiments, but results as I know them are shown in Table 6. Fig. 9 is a photograph of the experimental chamber of SATURN before shot 669. One can

Table 6. Samples of LMF First Wall Materials Irradiated SATURN X-Rays in May 1989

Sample No.	Shot No.	Material	Total X-ray Energy Fluence (J/cm^2)	Greater Than 900 eV Energy Fluence (J/cm^2)	Pulse Width (ns)	Result
1	658	Graphite H-451 fine grained	1900	440	21	destroyed powder
2	658	alumina coated aluminum 6061	1900	440	21	survived
3	664	Graphnol fine grained graphite	1600	370	18	destroyed six pieces
4	665	Graphite A05 short random fibers in a carbon matrix	2200	510	13	destroyed nothing left
5	669	K-Karb 2-D woven graphite in a carbon matrix	3400	730	16	survived delaminated
6	669	Graphite CGW fine grained	3400	730	16	destroyed powder
7	669	Graphite AJT fine grained	3400	730	16	destroyed powder
8	669	Dunlop break-pad graphite fibers in a carbon matrix	3400	730	16	destroyed shredded

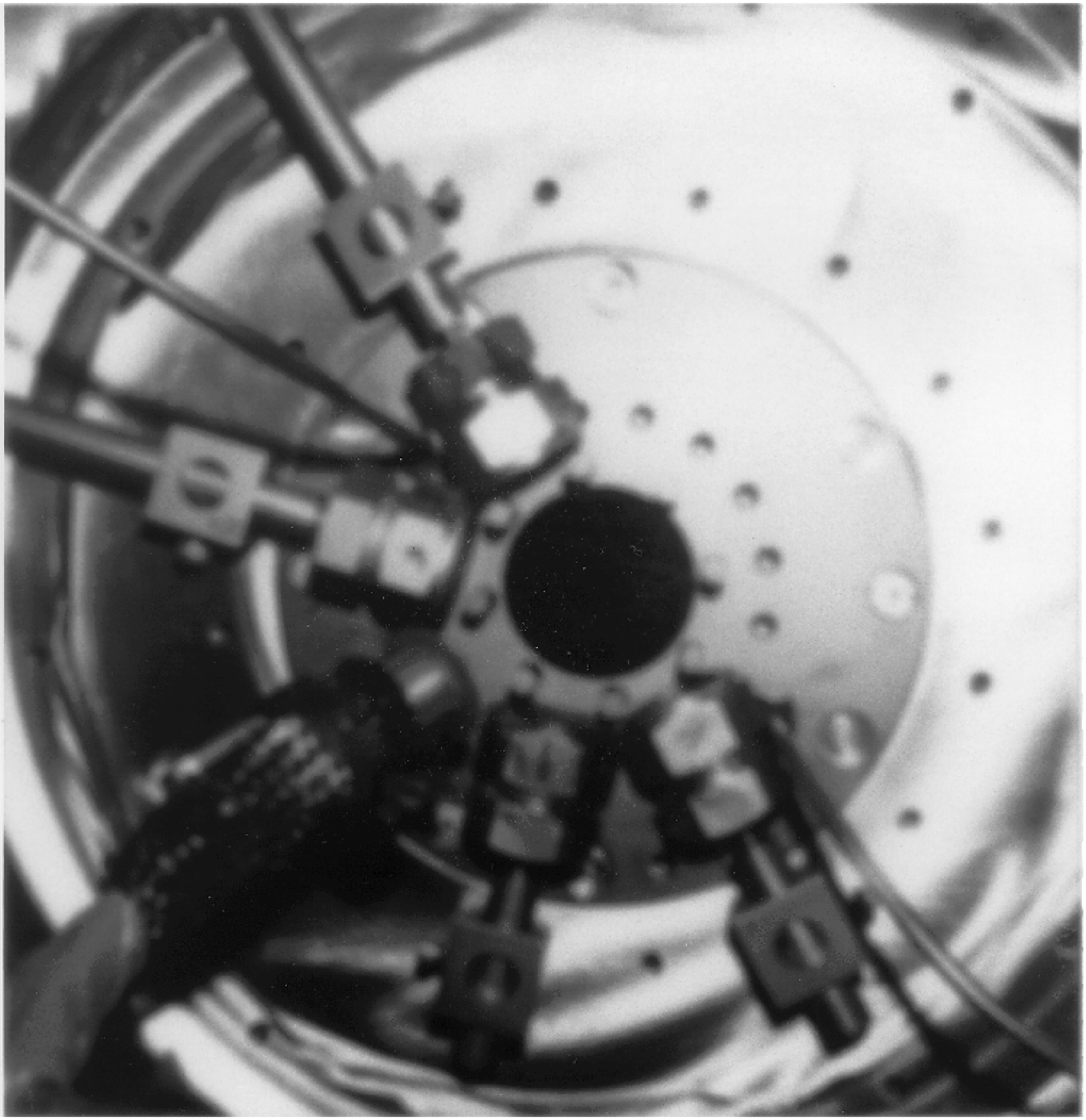

Fig. 9. Photograph of shot 669 on SATURN before shot. Samples 5, 6, 7, and 8 are in the four sample holders.

see the four sample holders that contain samples 5, 6, 7, and 8. The pinch is formed in the center of the dark circle in the middle of the photograph. The samples after they were irradiated with x-rays are shown in Fig. 10. One can see in Fig. 10 and in Table 6 that all samples except 2 and 5 were utterly destroyed. Sample 5, a two-directionally woven graphite in a carbon matrix called K-Karb, was not damaged in the plane of the graphite fibers but these planes became delaminated. Sample 2, aluminum 6061 with a layer of alumina blasted on its surface, survived well except that the alumina was removed. All of the other samples were fine grained graphites or graphites with short fibers. Sample 3, Graphnol, was a fine grained graphite that survived the best of these as it broke into about 6 pieces. The others were turned into powder. I could not even find any pieces of sample 4.

In August of 1989, I fielded another set of experiments on SATURN. These used argon gas pinches as an x-ray source. The spectra from these pinches differ from those for neon in the photon energy of the dominant lines: neon has lines at about 0.9 and 1.0 keV, while argon emits lines in the 3 to 4 keV range. Also, argon has about 40 kJ in these lines, while neon can have as much as 100 kJ in its lines. The pulse widths of the x-rays can be as low as 10 ns for argon gas pinches. For these experiments, I used 3 and 4 directionally woven graphites in a solid carbon matrix, bare aluminum 6061 and aluminum 6061 coated with a layer of carbon, a loose carpet material made of graphite, and two samples of 2-directionally woven graphite, where the x-rays were unfiltered and then filtered with a thin aluminum foil. The 3 and 4 directional graphites were an attempt to stop the delamination seen in K-Karb. The aluminum experiments are an extension of the previous experiments with alumina on aluminum in that they use a sacrificial layer to protect the aluminum, while carbon would be much easier to spray onto the wall of an LMF before each shot. The carbon carpet is a relatively new idea for LMF target chamber wall protection [13],

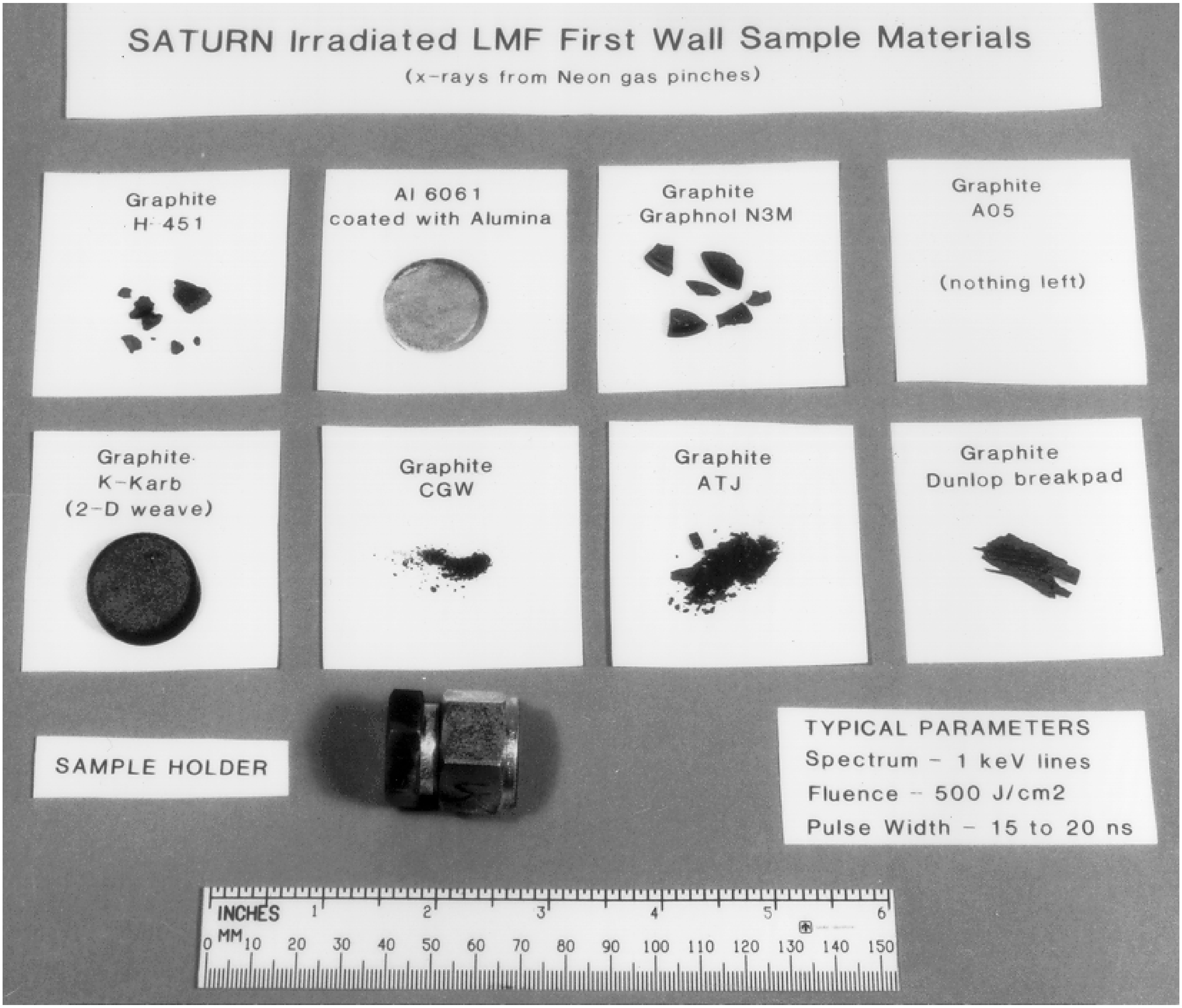

Fig. 10. Photograph of eight samples shot on Saturn during May 1989.

which uses the looseness of a long fibered carpet to prevent the generation of a shock. The filtering of x-rays is an experimental test of the low energy photon effects examined computationally.

The results of these experiments are given in Table 7. One can see that the aluminum survived both with and without the carbon protection. The 4-directional weave was successful in combating delamination, though the 3-directional random weave was not. The graphite carpet was almost totally undamaged by the x-rays. The unfiltered 2-directional weave was destroyed, while the filtered sample survived. I have no quantitative results yet as to the performance of the gas pinches, but preliminary indications are that there were in excess of 350 kJ of x-rays on all shots.

Table 7. Samples of LMF First Wall Materials Irradiated with SATURN X-Rays in August 1989

Sample #	Shot #	Material	Result
1	736	Bare aluminum 6061	survived
2	736	Carbon coated aluminum 6061	survived
3	736	Stapleknit graphite	destroyed delaminated
4	737	4-D woven graphite (FMI)	survived
5	739	3-D random fiber graphite	destroyed
6	737	A05 graphite fine grained	survived
7A	739	2-d woven graphite (unfiltered)	destroyed
7B	739	2-d woven graphite (filtered)	survived
8	737	Graphite carpet	survived

I should reemphasize here that this work is in progress. Several of the numbers quoted in Table 7 are still preliminary. I am still working on the fluences and spectra for these shots. I have done no post-shot analysis of the samples yet. I plan to study those that survived with a scanning electron microscope to see if the shocks caused any changes to the materials. I need to run computer simulations for the exact fluence and pulse width parameters for each sample, once they are well established.

4. FRAGMENTATION AND SHRAPNEL

A topic related to x-ray vaporization of first wall material is x-ray generated fragmentation of other structures in target chambers and the acceleration of such fragments into shrapnel. I have coupled some analytic models of fragmentation with the x-ray generated shock formalism of Section 2.1 to develop a means of estimating the size and speed of the shrapnel fragments. I then have estimated the shrapnel parameters for two types of structures that could be in the target chamber. I have not yet estimated the effects of the resulting shrapnel on the target chamber wall.

4.1 Analytic Treatment

I have chosen to think of the fragmentation as a two step process: 1) x-rays generate a large pressure gradient in the material which causes the material to move, and 2) this motion provides kinetic energy, some of which can be converted into the surface energy required for fragmentation. Step 1 can be modeled by the the method described in Section 2.1. For step 2, I have used the methods of Dennis Grady of SNL [14].

The pressure on a piece of material normal to the direction of the x-rays can be estimated from Eqn. 3. To obtain the proportionality constant C, one can compare with computer simulations. For example, if the material is graphite and one compares with CONRAD simulations for the LMF [15], C = 0.38. One can also compare with experiment. For a recently published x-ray vaporization experiment for aluminum, where the x-rays were created with lasers [16], $C = 0.35$. If the material is not normal to the x-rays, one must reduce the effective I_x by a factor of $\sin \alpha$, where α is the angle between the direction of the x-rays and the surface of the material. The deposition length is also affected by non-normal irradiation and is reduced by a factor of $\sin \alpha$. Therefore, the deposition rate per unit volume is independent of α and from this we have assumed that C_s is also independent of α. Therefore, as long as the deposition length is less than $C_s \delta t$, the pressure is proportional to $\sin \alpha$ and for graphite,

$$P = .38\, I_x \sin \alpha / C_s\,. \tag{6}$$

We can easily calculate the velocities of the shrapnel fragments by conservation of momentum. If the thickness of the material is T and the mass density is ρ, its areal mass density is ρT. The impulse is $P\, \Delta t$, which is the momentum gained by the material. Therefore, the velocity of the material is independent of the size of fragments it is broken into and can be expressed as,

$$v_{frag} = .38\, I_x \sin \alpha\, \Delta t / \rho T. \tag{7}$$

Finally, we must calculate the sizes of the fragments. The Grady model allows some of the kinetic energy about the center-of-mass of a piece of material that is to become a fragment to be converted into the surface energy of the fragment. For a solid, this model predicts that the average diameter of a fragment is

$$d = 2.72\, (K_{Ic} / \rho \dot{\varepsilon}\, C_s)^{2/3}\,. \tag{8}$$

Here, K_{Ic} is the fracture toughness, which for graphite is between 3×10^8 and 3×10^9 dyne / $cm^{3/2}$. The larger value is more conservative because it will lead to larger, more damaging shrapnel.

4.2. Typical Results

I have used this formalism to consider the fragmentation into shrapnel of two different structures. Both structures are assumed to be in an LMF target chamber where they are subjected to x-rays from a 1000 MJ target microexplosion. For a 1000 MJ target microexplosion and a graphite material, Eqn. 6 becomes

$$P = 4.96 \times 10^7 \sin\alpha/R \quad \text{(MPa)}\ , \tag{9}$$

where R is the distance between the target and the structure in cm. The fragment velocity then becomes,

$$v_{frag} = 2.16 \times 10^5 \sin\alpha/T\ R \quad \text{(cm/s)}\ , \tag{10}$$

where T is in cm.

First I considered a sphere of graphite concentric with the target. For a sphere, α is 90° and the strain rate is

$$\dot{\varepsilon} = 2\ v_{frag} / 3\ R\ . \tag{11}$$

Therefore, I can write the fragment diameter as

$$d = 4.53 \times 10^{-7}\ R^2\ T^{2/3} \quad \text{(cm)}\ . \tag{12}$$

I have tabulated some results in Table 8 for a graphite sphere, with T = 0.1 cm and for R from 10 to 100 cm. In addition to the fragment velocities and diameters, I show the fragment mass, M_{frag}, and momentum, Mom_{frag}. Notice that the momentum of each fragment increases with distance from the target.

The second structure we considered was a hollow graphite cylinder pointed directly at the target. Here, sin α is not constant, but is a function of the tube's radius and the distance that part of the tube is from the target,

$$\sin\alpha = r_{tube} / (\ r_{tube}^2 = R^2)^{1/2}\ . \tag{13}$$

Table 8. Fragment Parameters for a Sphere of Graphite Concentric with Targets in LMF Target Chamber

R (cm)	V_{frag} (m/s)	d (cm)	M_{frag} (g)	Mom_{frag} (g-cm/s)
10	2130	$1.0x10^{-5}$	$9.6x10^{-15}$	$2.0x10^{-9}$
20	1070	$3.9x10^{-5}$	$5.8x10^{-13}$	$6.2x10^{-8}$
50	430	$2.4x10^{-4}$	$1.3x10^{-10}$	$5.6x10^{-6}$
100	213	$1.0x10^{-3}$	$9.6x10^{-9}$	$2.0x10^{-4}$

I am assuming that the tube's radius, r_{tube}, is greater than the target radius, so that we can treat the target as a point source of x-rays. This insures that the x-rays will deposit on the inside surface of the tube and the tube will fragment due to rapid outward expansion. The pressure driving this expansion is, if R >> r_{tube},

$$P = 4.96 \times 10^7 \, r_{tube} / R^2 \quad \text{(MPa)} . \tag{14}$$

The velocity at which the tube cylindrically expands is,

$$v_{frag} = 2.16 \times 10^5 \, r_{tube} / T\, R^2 \quad \text{(cm/s)} . \tag{15}$$

For a cylindrical expansion, the strain rate is,

$$\dot{\varepsilon} = v_{frag} / 3\, r_{tube} . \tag{16}$$

Combining Eqn. 16 with Eqn. 8, we obtain the fragment diameter,

$$d = 7.18 \times 10^{-3}\, T^{2/3}\, R^2 \quad \text{(cm)} . \tag{17}$$

I have tabulated, for r_{tube} = 1 cm and T = 0.01 cm, the pressure, and the fragment speed, diameter, mass, and momentum in Table 9. Once again, one will notice that the momentum of a fragment increases as the distance from the target. The fragment speed falls of rather quickly because of the variation in sin α.

Table 9. Fragment Parameters for Graphite Tube in LMF Target Chamber

R	10 cm	20 cm	50 cm	100 cm	150 cm
P (GPa)	496	124	20	5.0	2.2
V_{frag} (m/s)	2160	540	86	22	9.6
d (cm)	0.033	0.133	0.833	*	*
M_{frag} (mg)	0.36	22.8	5578	*	*
Mom_{frag} (g-cm/s)	77	1232	4.8×10^4	*	*

*Fragment sizes are so large that model is no longer valid

5. SUMMARY AND CONCLUSIONS

I have used a simple scaling law and computer simulations to show that target x-rays will generate shocks in the first surfaces of unprotected LMF target chamber walls whose strength depends on the x-ray fluence, power intensity, and fluence. I have shown that gas pinches on the SATURN electron accelerator can provide x-rays that are relevant to some LMF concepts. I have performed preliminary experiments on SATURN that have shown bare aluminum, aluminum coated with a thin layer of alumina or graphite, four-directionally woven graphite, and graphite carpet all survive a single pulse of x-rays. I have begun to study the effects of low energy photons in the experiments done on graphite. I have considered the generation of shrapnel from structures internal to the LMF target chamber by the target x-rays.

Several issues need to be studied before a first wall material is chosen for the LMF. The experimental results reported in this paper are still preliminary in nature and much more data is needed. Samples need to be analyzed with electron or optical microscopy. The changes in material properties, such as elastic modulus and yield strength, brought about by the shocks need to be measured. Samples need to be repetitively irradiated with x-rays to study how the changes in properties will affect the response to shocks. Additional computer simulations will be needed as more information on properties of the material is obtained. The effect of debris in the SATURN experimental chamber needs to be addressed as does damage to the samples not related to the passage of shocks. Finally the techniques developed in this project should be applied to other materials that may be more relevant to ICF power plant designs.

Acknowledgement

This work was supported by Sandia National Laboratories and Lawrence Livermore National Laboratory. Computer simulations were performed on computers at SNL and both the experimental and computational work were performed while the author was on an extended visit to SNL.

REFERENCES

1. U.S. Department of Energy Inertial Fusion Division, "LMF-Laboratory Microfusion Capability Study, Phase I Summary," DOE/DP-0069.
2. R.R. Peterson, "Gas Condensation Phenomena in Inertial Confinement Fusion Reaction Chambers," Laser Interaction and Related Plasma Phenomena, vol. 7 (Plenum Press, New York, 1986), H. Hora and G. Miley, editors.
3. Ya.B. Zel'dovich and Yu.P. Raizer, "Physics of Shock Waves and High Temperature Hydrodynamic Phenomena," Academic Press, New York, 1967.
4. "LASL Shock Hugoniot Data," Stanley P. Marsh, editor (University of California Press, Berkeley, California, 1980).
5. F. Biggs and R. Lighthill, "Analytic Approximations for X-ray Cross Sections III," Sandia National Laboratories Report SAND87-0070 (August 1988).
6. J.J. MacFarlane, "IONMIX - A Code for Computing the Equation of State and Radiative Properties of LTE and Non-LTE Plasma," University of Wisconsin Fusion Technology Institute Report UWFDM-750 (December 1987).
7. R.R. Peterson, J.J. MacFarlane, and G.A. Moses, "CONRAD - A Combined Hydrodynamics - Condensation/Vaporization Computer Code," University of Wisconsin Fusion Technology Institute Report UWFDM-670 (January 1986, revised July 1988).
8. S.L. Thompson and J.M. McGlaun, "CSQIII An Eularian Finite Difference Program for Two-Dimensional Material Response: Users Manual," Sandia National Laboratories Report SAND87-2763 (January 1988).
9. C.L. Olson, "Achromatic Magnetic Lens Systems for High Current Ion Beams," Proceedings of the 1988 Linear Accelerator Conference, Williamsburg, VA, October 3-7, 1988, to be published.

10. G.A. Moses, R.R. Peterson, M.E. Sawan, and W.F. Vogelsang, "High Gain Target Spectra and Energy Partitioning for Ion Beam Reactor Design Studies," University of Wisconsin Fusion Technology Institute Report UWFDM-396 (1980).

11. R.B. Spielman, et al., "Efficient X-ray Production From Ultrafast Gas-Puff Z Pinches," J. Appl. Phys. 57, 830 (1985).

12. Progress Report: Narya Pulsed-Power-Driven X-ray Laser Program -- January 1984 through June 1985, M.K. Matzen, ed., SAND85-1151, Sandia National Laboratories, 1986.

13. M.J. Monsler and W.R. Meier, "A Carbon-Carpet First Wall for the Laboratory Microfusion Facility," Fusion Technology 15, 595 (1989).

14. D.E. Grady, "Local Inertial Effects in Dynamic Fragmentation," J. Appl. Phys. 53, 322 (1982).

15. B. Badger, et al., "Target Chamber Studies for a Light Ion Fusion Laboratory Microfusion Facility," University of Wisconsin Fusion Technology Institute Report UWFDM-768 (August 1988).

16. T. Endo, H. Shiraga, K. Shihoyama, and Y. Kato, "Generation of a Shock Wave by Soft - X-ray - Driven Ablation," Phys. Rev. Lett. 60, 1022 (1988).